

# Quasi-Invariants for Recognition of Articulated and Non-standard Objects in SAR Images

Grinnell Jones III and Bir Bhanu  
Center for Research in Intelligent Systems  
University of California, Riverside, CA 92521  
{grinnell, bhanu} @vislab.ucr.edu

## Abstract

*Using SAR scattering center locations and magnitudes as features, invariances with articulation (i.e., turret rotation for the ZSU 23/4 gun and T72 tank), with configuration variants (e.g. fuel barrels, searchlights, etc.) and with a depression angle change are shown for real SAR images obtained from the MSTAR public data. This location and magnitude quasi-invariance forms a basis for an innovative SAR recognition engine that successfully identifies real articulated and non-standard configuration vehicles based on non-articulated, standard recognition models. Identification performance results are given as confusion matrices and ROC curves for articulated objects, for configuration variants, and for a small change in depression angle.*

## 1. Introduction

In this paper we are concerned with the problem of recognizing articulated vehicles and actual vehicle configuration variants in real SAR images. Previous work on recognizing articulated objects in visual imagery [1] [4] used simple objects (like scissors and lamps) and employed constraints around a joint to recognize these objects. Because of the unique characteristics of SAR image formation (specular reflection, multiple bounces, low resolution and non-literal nature of the sensor), it is difficult to extract linear features (commonly used in visual images), especially from subcomponents of vehicle size objects in SAR images at one foot resolution. Prior recognition methods for SAR imagery using templates [9] [10], are not well suited for recognition of articulated objects, because each different articulation configuration requires a different template leading to a combinatorial explosion. Prior detection theory [3],

pattern recognition [10], and neural network [11] approaches to SAR recognition all tend to use global features that are optimized for standard, non-articulated, non-occluded configurations, however, articulation and occlusion often change global features (e.g. the object outline and major axis).

Our approach to object recognition is specifically designed for SAR images. In contrast to passive vision systems, the scale of the image is fixed in SAR by characteristics of the radar. However, where optical images are mainly formed as a result of diffuse reflections from a noncoherent source of light, SAR images are formed primarily from specular reflections from a coherent source; they are non-literal and vary quickly and abruptly with small pose angle variations. Because of the high SAR image variance with object pose, or azimuth (the radar depression angle to the target is known), we use 360 azimuth models at  $1^\circ$  intervals of each object in a standard non-articulated configuration for recognizing articulated and non-standard versions of these same objects (in contrast to others who have used  $5^\circ$  to  $10^\circ$  intervals [5] [10] for recognizing standard non-articulated objects). The peaks (local maxima) in radar return are related to the physical geometry of the object. The relative locations of these scattering centers are independent of translation and serve as distinguishing features.

We approach the problem of recognizing articulated and occluded objects from the fundamentals of SAR images. We identify (and measure) the invariance of SAR scatterer locations and magnitudes with object articulation, configuration variants and a small change in depression angle. Based on these invariants, we develop a SAR specific recognition system that uses standard non-articulated recognition models to successfully recognize articulated and non-standard versions of these objects. The SAR recognition engine has an off-line model construction phase and an on-line recognition process. The recognition model is basically a

look-up table that relates relative distances among the scattering centers (in the radar range and cross range directions) to object type and azimuth. The recognition process is an efficient search for *positive evidence*, using relative locations of scattering centers in the test image to access the look-up table and generate votes for the appropriate object, pose (azimuth) and translation. The approach accommodates a ‘within one pixel’ uncertainty in the locations of the scattering centers. A constraint on allowable percent change in the magnitudes of the data and model scattering centers is used to help filter out false matches. Identification performance results are given as confusion matrices and ROC curves for articulated objects, for configuration variants, and for a small change in depression angle.

The key contributions of this paper are:

1. Demonstrates that quasi-invariant scattering center *locations* exist and that their *magnitudes* are also quasi-invariant for (a) articulation; (b) configuration variants; and (c) a depression angle change for actual vehicles in real SAR data.
2. Develops a new recognition engine based on scattering center location and magnitude features that achieves significant vehicle recognition performance for articulation, configuration variants and depression angle changes with real SAR data.

## 2. Scatterer Location Invariance

The relative locations of SAR scattering centers, determined from local peaks in the radar return, are related to the aspect and physical geometry of the object, independent of translation and serve as distinguishing features. Photo images of typical MSTAR targets: T72 tank serial number (#) a64 and ZSU 23/4 anti-aircraft gun #d08, are shown in Figures 1 and 2, both with the turret in the straight forward and articulated positions. Regions of interest (ROI) are found in the MSTAR SAR target chips by reducing speckle noise using the Crimmins algorithm in Khoros [7], thresholding at the mean plus two standard deviations, dilating to fill small gaps among regions, eroding to have one large ROI and little regions, discarding the small regions with a size filter and dilating to expand the extracted ROI. The scattering centers are extracted from the SAR magnitude data (within the boundary contour of the ROI) by finding local eight-neighbor maxima. Example SAR images and the regions of interest (ROI), with the locations of the scattering centers superimposed, are shown in Figure 3 for baseline (turret straight) and articulated (turret at 315°) versions of the ZSU 23/4. Because the object and ROI are not registered, we express



(a) turret straight.



(b) turret articulated.

**Figure 1. T72 tank #a64.**

the scattering center location invariance with respect to articulation, configuration differences or depression angle changes as the maximum number of corresponding scattering centers (whose locations match within a stated tolerance) for the optimum integer pixel translation.

Given an original version of a SAR target image with  $n$  scattering centers, represented by points at pixel locations  $P_i = (x_i, y_i)$  for  $1 \leq i \leq n$  and a translated, distorted version  $P'_j = (x'_j, y'_j)$  ( $1 \leq j \leq n$ ) at a translation  $t = (t_x, t_y)$ , we define a *match* between points  $P'_j$  and  $P_i$  as:

$$M_{ij}(t) = \begin{cases} 1 & \text{if } |x'_j - t_x - x_i| \leq l \text{ and} \\ & |y'_j - t_y - y_i| \leq l \\ 0 & \text{otherwise} \end{cases}$$

where  $l = 0$  for an ‘exact’ match and  $l = 1$  for a match ‘within one pixel’.

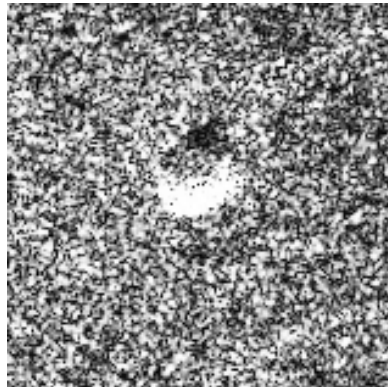


(a) turret straight.

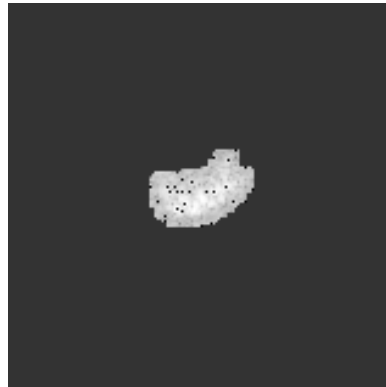


(b) turret articulated.

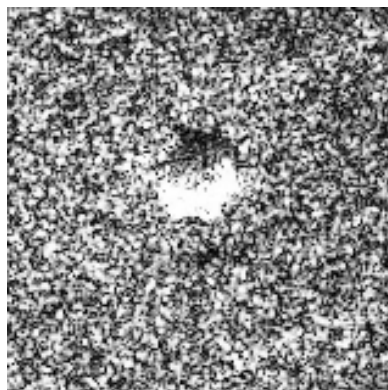
**Figure 2. ZSU 23/4 gun #d08.**



(a) baseline image.



(b) baseline ROI.



(c) articulated image.



(d) articulated ROI.

**Figure 3. MSTAR SAR images and ROIs (with peaks shown as +) for ZSU 23/4 gun #d08 at 66° hull azimuth.**

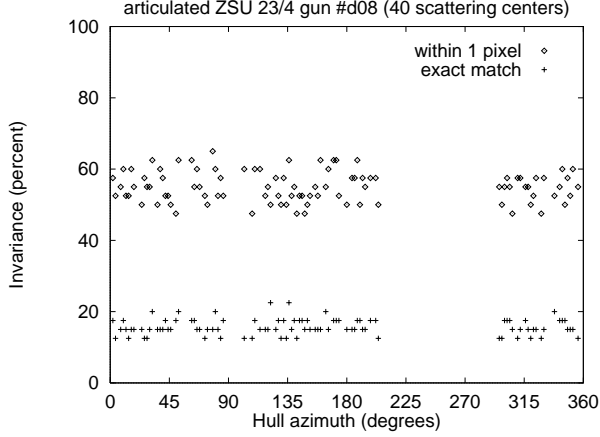


**Figure 4. Articulated ZSU 23/4 gun scatterer location invariance.**

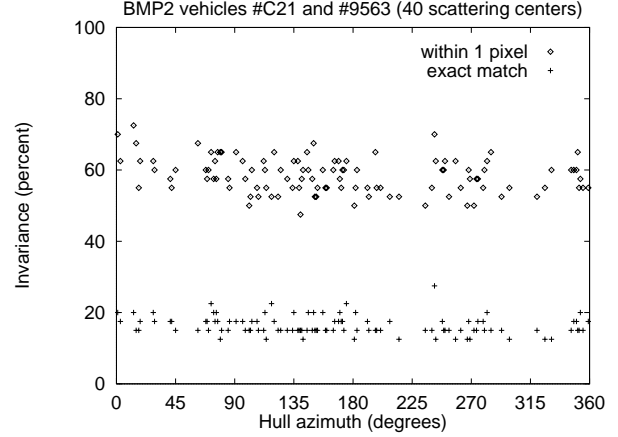


**Figure 5. BMP2 scatterer location invariance with configuration (#C21 vs. #9563).**

The scatterer location invariance,  $L_n$ , of  $n$  scatterers, expressed as a percentage of matching points, is given by:

$$L_n = \max_t \left\{ \frac{100}{n} \sum_{j=1}^n \min \left( \left( \sum_{i=1}^n M_{ij}(t) \right), 1 \right) \right\}$$

where each point  $P'_j$  is restricted to at most one match.

Figure 4 shows the location invariance,  $L_{40}$ , of the strongest 40 scattering centers with articulation for MSTAR ZSU 23/4 #d08 (at a  $30^\circ$  depression angle) as a function of the hull azimuth. The average invariance is 15.7% for an exact match of scattering centers and 55.1% for a location match within a one pixel ( $3 \times 3$  neighborhood) tolerance. Similarly, Figure 5 shows the percent of the strongest 40 scattering center locations that are invariant for BMP2 vehicle #C21 vs. #9563 (at a  $15^\circ$  depression angle). Figure 6 shows the percent scattering center location invariance for BMP2 #C21 at  $17^\circ$  vs.  $15^\circ$  depression angles. The mean and standard deviation for percent location invariance (for 40 scatterers, and depression angle  $\phi$ ) are shown in Table 1 for articulated versions of the T72 and ZSU 23/4, for configuration variants of the T72 and BMP2 and for depression angle changes with the T72 and BMP2.

The mean 17.17% exact match location invariance with articulation for the real MSTAR T72 #a64 (at one foot resolution) is significantly less than the comparable 46.6% invariance (reported by Jones and Bhanu [6]) for T72 SAR signatures generated with the XPATCH radar signature prediction code at six inch resolution. Similarly, the two real articulated objects in the MSTAR data had an average 16.45% location invariance in Table 1, compared with a 49% invariance

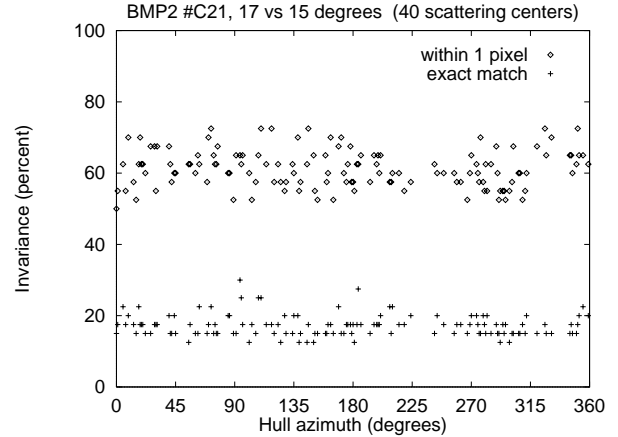


**Figure 6. BMP2 #C21 scatterer location invariance with depression angle  $17^\circ$  vs.  $15^\circ$ .**

**Table 1. Scatterer percent location invariance for MSTAR targets with articulation, configuration variants and depression angle changes.**

	dep. angle	exact match invariance		within 1 pixel invariance	
		mean	s. d.	mean	s. d.
articulation:					
T72 #a64	30	17.17	1.47	57.83	2.23
ZSU #d08	30	15.69	0.91	55.05	1.72
average		16.45		56.47	
configuration variants:					
T72: #812 vs #132	15	15.34	0.89	55.34	1.91
#s7 vs #132	15	15.40	0.83	56.68	1.95
BMP2: #9563 vs #c21	15	16.34	0.84	58.52	1.97
#9566 vs #c21	15	16.17	0.99	57.93	1.97
average		15.83		57.15	
depression angle:					
T72 #132	17-15	17.76	1.52	61.55	2.05
BMP2 #c21	17-15	17.19	1.23	61.31	2.11
average		17.47		61.43	

for four XPATCH generated articulated objects (at six inch resolution).

### 3. Scatterer Magnitude Invariance

Using a scaled scatterer amplitude (S), expressed as a radar cross section in square meters, given by  $S = 100 + 10 \log_{10}(i^2 + q^2)$ , where  $i$  and  $q$  are the components of the complex radar return, we define a percent amplitude change ( $A_{jk}$ ) as:  $A_{jk} = 100(S_j - S_k)/S_j$ . (This form allows a larger variation for the stronger signal returns.) A location and magnitude match  $Q_{jk}(t)$  is given by:

$$Q_{jk}(t) = \begin{cases} 1 & \text{if } M_{jk}(t) = 1 \text{ and } |A_{jk}| \leq l_A \\ 0 & \text{otherwise} \end{cases}$$

where  $l_A$  is the percent amplitude change tolerance. The scatterer magnitude and location invariance ( $I_n$ ), expressed as a percentage of  $n$  scatterers, is given by:

$$I_n = \max_t \left\{ \frac{100}{n} \sum_{k=1}^n \min \left( \left( \sum_{j=1}^n Q_{jk}(t) \right), 1 \right) \right\}$$

Figure 7 shows the probability mass functions (PMFs) for percent amplitude change for the strongest 40 articulated vs. non-articulated scattering centers of ZSU 23/4 #d08. Curves are shown both for the cases where the scattering center locations correspond within a one pixel tolerance and for all the combinations of scatterers whose locations do not match. For the cases with locations that matched within 1 pixel, the percent amplitude change mean and standard deviation are 0.06 and 7.44, while the non-matching cases are 0.08 and 11.37 respectively. The crossover points of the two curves are at  $\pm 9$  percent. Similarly, Figure 8 shows the PMFs for percent amplitude change for the strongest 40 scattering centers of BMP2 #C21 vs. #9563 (at a  $15^\circ$  depression angle), while Figure 9 shows this for  $17^\circ$  vs.  $15^\circ$  degrees depression angle (for BMP2 #C21). The mean and standard deviation for these matching and non-matching scatterers and the crossover points for the PMFs are given in Table 2. Table 3 shows the mean and standard deviation for the percent location and magnitude invariance (within a 1 pixel location tolerance and an amplitude change tolerance of  $l_A$ ) of the strongest 40 scatterers for these same articulation, configuration difference and depression angle change cases.

### 4. SAR Recognition Engine

The SAR recognition engine uses standard non-articulated models of the objects (at  $1^\circ$  azimuth incre-

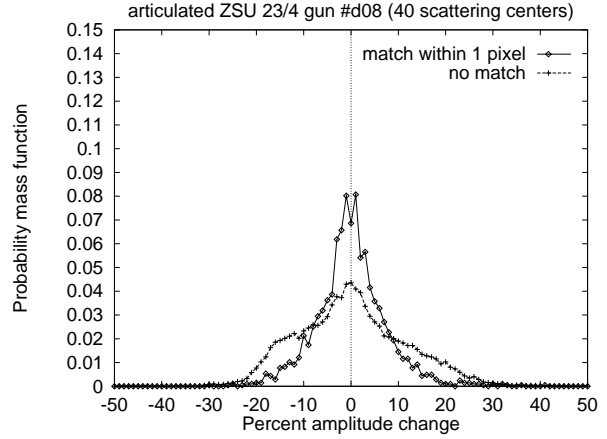


Figure 7. ZSU 23/4 scatterer percent amplitude change with articulation.

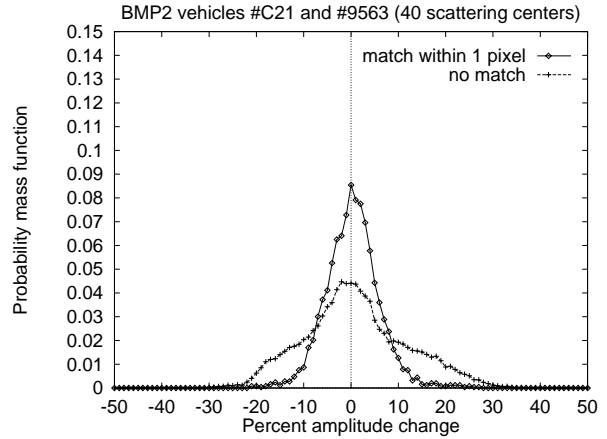


Figure 8. Example BMP2 scatterer percent amplitude change with configuration (#C21 vs. #9563).

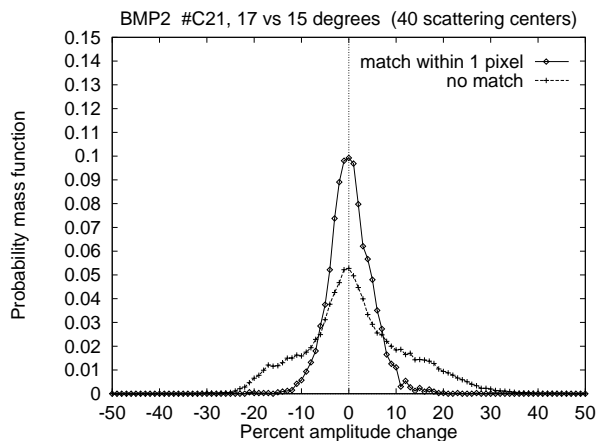


Figure 9. BMP2 scatterer percent amplitude change with depression angle 17° vs. 15°.

Table 2. Scatterer percent amplitude change for MSTAR targets with articulation, configuration variants and depression angle changes.

	within 1 pixel		no match		x-over
	mean	s. d.	mean	s. d.	
articulation:					
T72 #a64	.51	5.91	.75	10.44	-5/+6
ZSU #d08	.06	7.44	.08	11.37	±9
configuration variants:					
T72: #812 vs #132	.15	7.29	-.38	11.12	±8
#s7 vs #132	.48	6.69	2.20	11.15	±9
BMP2: #9563 vs #c21	.35	5.72	.94	10.88	-8/+9
#9566 vs #c21	.48	6.20	.56	10.68	-7/+8
depression angle:					
T72 #132	.43	4.66	.84	10.45	-7/+8
BMP2 #c21	.37	4.65	1.53	10.91	-7/+8

Table 3. Scatterer percent location and magnitude invariance (for locations within one pixel and amplitude tolerance  $l_A$ ).

	$l_A$	mean	s. d.
articulation:			
T72 #a64	±9	53.47	2.63
ZSU #d08	±9	47.98	2.22
average		50.78	
configuration variants:			
T72: #812 vs #132	±9	48.40	2.42
#s7 vs #132	±9	50.69	2.44
BMP2: #9563 vs #c21	±9	54.38	2.34
#9566 vs #c21	±9	53.00	2.51
average		51.68	
depression angle:			
T72 #132	±7	56.15	2.38
BMP2 #c21	±7	55.66	2.53
average		55.91	

ments) to recognize the same objects in non-standard, articulated and occluded configurations. The current 6D model-based SAR recognition engine, described here, is an outgrowth of our earlier 2D SAR engine (that approach only used the relative locations; it did not determine the appropriate translation or utilize the magnitude information). The model construction algorithm is outlined in Figure 10 and the recognition algorithm is given in Figure 11. Using a technique like geometric hashing, [8] the relative positions of the scattering centers in the range (R) and cross-range (C) directions are the (initial 2D) indices to a look-up table of labels that give the associated target type/pose and the remaining 4D features: range and cross-range position of the ‘origin’ and the magnitudes of the two scatterers. (The ‘origin’ is the strongest of a pair of scatterers, the other is a ‘point’.) In comparing the test data with the model, the additional 4D information provides results on the range and cross-range translation and the percent magnitude changes for the two scattering centers. The number of scattering centers used, the limits on allowable translations and the limits on allowable magnitude changes are design parameters that are optimized, based on experiments, to produce the best forced recognition results.

The recognition process is an efficient search for positive evidence, using relative locations of scattering centers to access the look-up table and generate votes for the appropriate object, azimuth, range and cross range

1. For each model Object do 2
2. For each model Azimuth do 3, 4, 5
3. Obtain the location ( $R, C$ ) and magnitude ( $S$ ) of the strongest M scatterers.
4. Order ( $R, C, S$ ) triples by descending  $S$ .
5. For each origin O from 1 to M do 6
6. For each point P from O+1 to M do 7, 8
7.  $dR = R_P - R_O$ ;  $dC = C_P - C_O$ .
8. At look-up table location  $dR, dC$  append to list entry with: Object, Azimuth,  $R_O, C_O, S_O, S_P$ .

**Figure 10. Model construction algorithm**

1. Obtain from test image the location ( $R, C$ ) and magnitude ( $S$ ) of M strongest scatterers.
2. Order ( $R, C, S$ ) triples by descending  $S$ .
3. For each origin O from 1 to M do 4
4. For each point P from O+1 to M do 5, 6
5.  $dR = R_P - R_O$ ;  $dC = C_P - C_O$ .
6. For DR from  $dR-1$  to  $dR+1$  do 7
7. For DC from  $dC-1$  to  $dC+1$  do 8, 9, 10
8.  $\text{weighted\_vote} = |\text{DR}| + |\text{DC}|$ .
9. Look up list of model entries at DR, DC.
10. For each model entry  $E$  in the list do 11
11. IF  $|\text{tr} = R_O - R_E| < \text{translation\_limit}$  and  $|\text{tc} = C_O - C_E| < \text{translation\_limit}$  and  $|1 - S_{EO}/S_O| < \text{magnitude\_limit}$  and  $|1 - S_{EP}/S_P| < \text{magnitude\_limit}$   
THEN increment accumulator array [Object, Azimuth, tr, tc] by  $\text{weighted\_vote}$ .
12. Query accumulator array for each Object, Azimuth, tr and tc, summing the votes in a 3x3 neighborhood in translation subspace about tr, tc; record the maximum vote\_sum and the corresponding Object.
13. IF maximum vote\_sum > threshold  
THEN result is Object ELSE result is "unknown".

**Figure 11. Recognition algorithm**

**Table 4. Example MSTAR articulated object confusion matrix (38 scatterers,  $\pm 9\%$  amplitude tolerance, 2100 vote threshold).**

MSTAR (Public) articulated test targets		Identification results [non-articulated models]		
		T72	ZSU	unknown
T72	315 <sup>0</sup> turret	98	0	0
ZSU	315 <sup>o</sup> turret	0	92	2
BRDM2	(confuser)	32	0	222

translation. A (city-block) weighted voting method is used to reduce the impact of the more common small relative distances. To accommodate some uncertainty in the scattering center locations, the eight-neighbors of the nominal range and cross-range relative location are also probed and the translation results are accumulated for a 3x3 neighborhood in the translation subspace. The process is repeated with different scattering centers as reference points, providing multiple ‘looks’ at the model database to handle spurious scatterers that arise due to articulation, occlusion or configuration differences.

To handle identification with ‘unknown’ objects, we introduce a criteria for the quality of the recognition result (e.g. the votes for the potential winning object exceed some threshold,  $v_{min}$ ). By varying the decision rule parameter (typically from 1000 to 4000 votes in 50 vote increments) we obtain a form of Receiver Operating Characteristic (ROC) curve with probability of correct identification (PCI) vs. probability of false alarm (PFA).

## 5. Recognition Results

### 5.1. Articulated Object Results

Table 4 shows recognition results for articulated versions of the T72 #a64 and ZSU23/4 #d08 at 30° depression angle, using the non-articulated versions of these same serial number objects as the models and BRDM2 #e71 as an “unknown” confuser vehicle. These results, 0.990 PCI at 0.126 PFA, are obtained using a 2100 vote decision criterion with 38 scatterers and with a  $\pm 9$  percent amplitude change limit. (The overall forced recognition rate is 100% over a range from 14 to 40 scattering centers.) For the conditions in Table 4, varying the vote threshold results in the ROC curve shown in Figure 12.

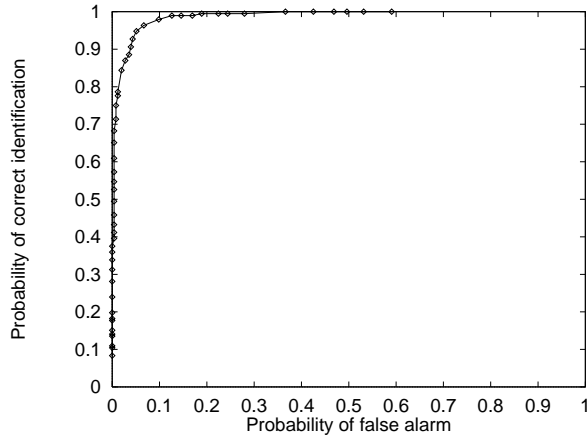


**Figure 12. Receiver Operating Characteristics for recognizing MSTAR articulation.**

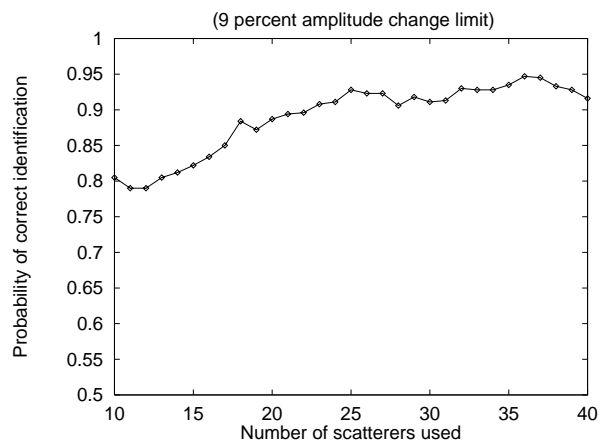
## 5.2. Configuration Variant Results

Table 5 shows a typical forced recognition confusion matrix for configuration variants in the MSTAR data at  $15^\circ$  depression angle, using a single configuration as the model (BMP2 #C21 and T72 #132) and testing with two other variants of each vehicle type. Although more extensive T72 configuration variant data is available, only two configurations are used so that the amount of test data for the T72 and BMP2 is comparable and the results are not artificially biased toward recognizing the T72. The optimum forced recognition result is an overall rate of 94.7%, obtained at 36 scattering centers with a translation limit of  $\pm 5$  pixels and a percent magnitude change of less than  $\pm 9$  percent. (The 94.7% rate for this 6D recognition engine is directly comparable to the 68.4% rate for the prior 2D version of the recognition engine.) The effect on PCI of the number of scattering centers used is shown in Figure 13 (for  $l_A = 9$ ) and Figure 14 shows the effect of varying the amplitude change limit (for 36 scattering centers). Using the BTR70 #c71 as an “unknown” confuser, for the optimum conditions given above, results in the ROC curve shown in Figure 15.

The effect of scatterer location and magnitude invariance on the forced recognition rate for configuration differences of the T72 and BMP2 is shown in Figure 16, based on the 22 failures in 415 tests shown in Table 5. (The two cases of perfect recognition below 35% are each a single instance with no failure.) These results with actual SAR data for the 6D recognition engine show over 90% recognition for location and magnitude invariance (within one pixel and an amplitude change tolerance of 9%) values down to 41.7%, compared to

**Table 5. Forced recognition confusion matrix for MSTAR configuration variants (36 scatterers,  $\pm 9\%$  amplitude tolerance).**

MSTAR (Public) test targets [serial number]	Identification results [configurations modeled]	
	BMP2 [#c21]	T72 [#132]
BMP2 [#9563]	106 (98.1%)	2
BMP2 [#9566]	107 (97.2%)	3
T72 [#812]	11	92 (89.3%)
T72 [#S7]	6	88 (93.6%)



**Figure 13. Effect of number of scattering centers used on recognition of MSTAR configuration differences.**

the prior results [6] for the 2D engine with simulated SAR data (at six inch resolution) where the recognition rate drops sharply below 40% invariance for an exact match of locations.

## 5.3. Depression Angle Change Results

Table 6 shows the confusion matrix for recognizing T72 (#132) and BMP2 (#c21) at a  $17^\circ$  depression angle using models with the same serial numbers at a  $15^\circ$  depression angle and using BTR70 #c71 as an “unknown” confuser. These results, 0.855 PCI at 0.129 PFA, are obtained using a threshold of 2100 votes with 34 scatterers and with an amplitude change limit of  $\pm 7\%$ . (The forced recognition rate is greater than 90% over a range of from 13 to at least 40 scatterers with the best forced recognition, 99.6%, at 34 scatterers with a  $\pm 7\%$  amplitude change limit.) The ROC curve for these depression angle changes is shown as Figure 17.

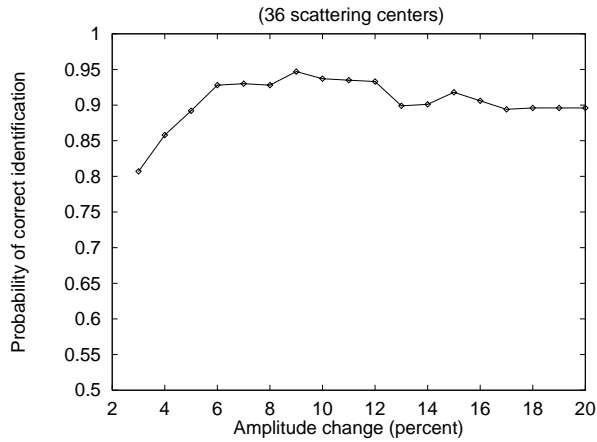


**Figure 14. Effect of amplitude change tolerance on recognition of MSTAR configuration differences.**

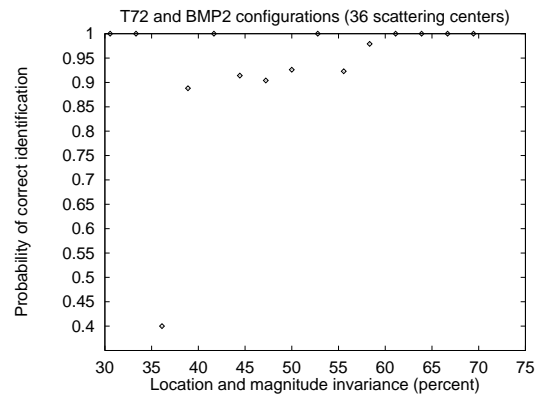


**Figure 16. Effect of location and magnitude invariance on forced recognition for MSTAR configuration differences.**

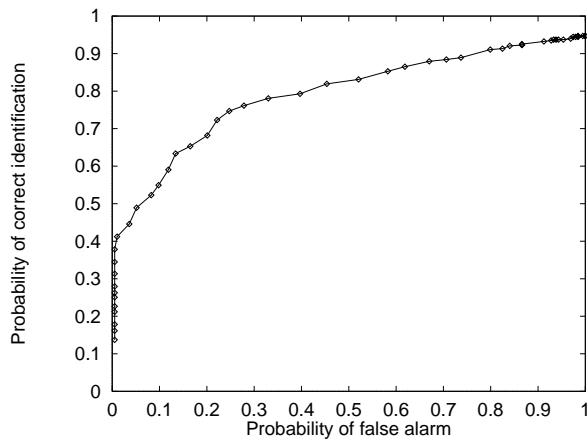


**Figure 15. Receiver Operating Characteristics for recognizing MSTAR configuration differences.**

**Table 6. Example confusion matrix for MSTAR depression angle changes (34 scatterers,  $\pm 7\%$  amplitude tolerance, 2100 vote threshold).**

MSTAR (Public) depression angle 17° test targets	Identification results [15° models]		
	BMP2	T72	unknown
BMP2 [#c21]	117	0	21
T72 [#132]	1	119	18
BTR70 (confuser)	10	20	202

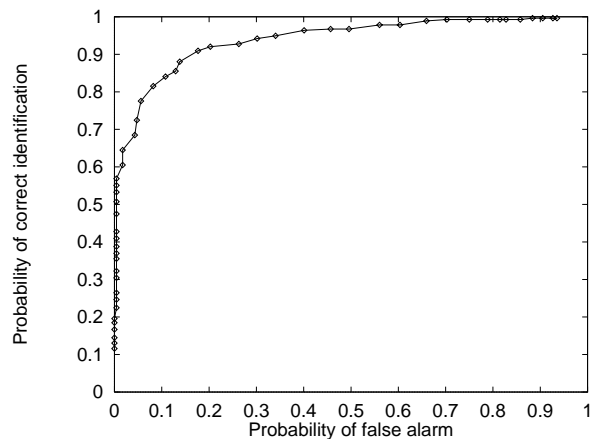


**Figure 17. Receiver Operating Characteristics for recognizing MSTAR depression angle changes.**

## 6. Conclusions and Future Work

A significant percentage (56.5 - 61.4%) of the SAR scattering center locations are quasi-invariant (within a 3x3 pixel tolerance) for object articulation, configuration differences and small depression angle changes. The magnitudes of these quasi-invariant scatterers (expressed as a radar cross section) typically change by less than  $\pm 10\%$ . The positions and magnitudes of pairs of these quasi-invariant scatterers are used in a 6D recognition engine to achieve good recognition results with real SAR data for object articulation, configuration differences and small depression angle changes. While these three problems are similar, the differences among configurations of an object type are a more significant challenge for recognition than articulation and depression angle changes, where the model and test data are the same physical object under different conditions (as seen by comparing the ROC curves in Figure 15 with Figures 12 and 17). These recognition results are a substantial improvement over the performance of the earlier 2D recognition approach with real SAR data [2]. Future work to incorporate additional features in the recognition engine should lead to further performance improvements and accommodate combined cases such as configuration variants along with depression angle changes.

## 7. Acknowledgements

This work was supported in part by grant F49620-97-1-0184; the contents and information do not reflect the positions or policies of the U.S. Government.

## References

- [1] A. Beinglass and H. Wolfson. "Articulated object recognition, or : How to generalize the generalized Hough transform," *Proc. IEEE Conf. on Computer Vision and Pattern Recognition*, pp. 461-466, June 1991.
- [2] B. Bhanu, G. Jones and J. Ahn. "Recognizing articulated objects and object articulation in synthetic aperture radar imagery," *SPIE Proceedings: Algorithms for Synthetic Aperture Radar Imagery V*, Orlando, FL, April 1998.
- [3] D. Casasent and R. Shenoy. "Detection and classification in SAR using MINACE correlation filters," *SPIE Proceedings: Algorithms for Synthetic Aperture Radar Imagery II*, Vol. 2487, pp. 211-224, Orlando, FL, April 1995.
- [4] Y. Hel-Or and M. Werman, "Recognition and localization of articulated objects," *Proc. IEEE Workshop on Motion of Non-Rigid and Articulated Objects*, pp. 116-123, Austin, TX, November 11-12, 1994.
- [5] K. Ikeuchi, T. Shakunga, M. Wheeler, and T. Yamazaki. "Invariant histograms and deformable template matching for SAR target recognition," *Proc. IEEE Conf. on Computer Vision and Pattern Recognition*, pp. 100-105, June 1996.
- [6] G. Jones and B. Bhanu. "Recognition of articulated and occluded objects," *IEEE Transactions on Pattern Analysis and Machine Intelligence*, in press.
- [7] *Khoros Pro v2.2 User's Guide*, Addison Wesley Longman Inc., 1998.
- [8] Y. Lamden and H. Wolfson. "Geometric hashing: A general and efficient model-based recognition scheme," *Proc. International Conference on Computer Vision*, pp. 238-249, December 1988.
- [9] L. Novak, G. Owirka, and C. Netishen, "Radar target identification using spatial matched filters." In *Pattern Recognition*, Vol. 27, No. 4, pp. 607-617, 1994.
- [10] J. Verly, R. Delanoy, and C. Lazott. "Principles and evaluation of an automatic target recognition system for synthetic aperture radar imagery based on the use of functional templates," *SPIE Proceedings: Automatic Target Recognition III*, vol 1960, pp. 57-71, Orlando, FL, April 1993.
- [11] A. Waxman, M. Seibert, A. Bernardon, and D. Fay. "Neural systems for automatic target learning and recognition," *The Lincoln Laboratory Journal*, Vol. 6, No. 1, pp. 77-116, 1993.